

Spin-orbit-controlled metal-insulator transition in Sr_2IrO_4

B. Zwartsenberg,^{1,2} R.P. Day,^{1,2} E. Razzoli,^{1,2} M. Michiardi,^{1,2,3} N. Xu,⁴ M. Shi,⁴ J.D. Denlinger,⁵ S. Calder,⁶ K. Ueda,⁷ J. Bertinshaw,⁷ H. Takagi,⁷ B.J. Kim,^{8,7} I.S. Elfimov,^{1,2} and A. Damascelli^{1,2}

¹Quantum Matter Institute, University of British Columbia, Vancouver, BC V6T 1Z4, Canada

²Department of Physics and Astronomy, University of British Columbia, Vancouver, BC V6T 1Z1, Canada

³Max Planck Institute for Chemical Physics of Solids, Nöthnitzer Straße 40, 01187 Dresden, Germany

⁴Swiss Light Source, Paul Scherrer Institut, CH-5232 Villigen PSI, Switzerland

⁵Advanced Light Source, Lawrence Berkeley National Laboratory, Berkeley, California 94720, USA

⁶Quantum Condensed Matter Division, Oak Ridge National Laboratory, Oak Ridge, Tennessee 37831, USA

⁷Max Planck Institute for Solid State Research, Heisenbergstraße 1, 70569 Stuttgart, Germany

⁸Department of Physics, Pohang University of Science and Technology, Pohang 790-784, South Korea

(Dated: February 6, 2019)

In the context of correlated insulators, where electron-electron interactions (U) drive the localization of charge carriers, the metal-insulator transition (MIT) is described as either bandwidth (BC) or filling (FC) controlled [1]. Motivated by the challenge of the insulating phase in Sr_2IrO_4 , a new class of correlated insulators has been proposed, in which spin-orbit coupling (SOC) is believed to renormalize the bandwidth of the half-filled $j_{\text{eff}} = 1/2$ doublet, allowing a modest U to induce a charge-localized phase [2, 3]. Naturally, the question arises whether in this new framework the MIT can be driven by SOC. Previous attempts at revealing the role of SOC [4, 5] have been hindered by concurrently occurring changes to the filling [6–8]. We overcome this challenge by employing multiple substituents that introduce well defined changes to the signatures of SOC and carrier concentration in the electronic structure, as well as a new methodology that allows us to monitor SOC directly. Specifically, we study $\text{Sr}_2\text{Ir}_{1-x}\text{T}_x\text{O}_4$ ($\text{T} = \text{Ru}, \text{Rh}$) by angle-resolved photoemission spectroscopy (ARPES) combined with *ab-initio* and cluster tight-binding calculations. This allows us to distinguish relativistic and filling effects, thereby establishing conclusively the central role of SOC in stabilizing the insulating state of Sr_2IrO_4 . Most importantly, we determine the critical value for spin-orbit coupling for this system to be $\lambda_c = 0.41$ eV, and provide the first demonstration of a spin-orbit-controlled MIT.

The familiar tools of chemical doping and pressure have provided straightforward access to both FC and BC MIT in conventional correlated insulators. In an effort to unveil the role of SOC in the insulating behavior of Sr_2IrO_4 , and whether it can indeed drive a MIT, we have attempted to controllably dilute SOC in the valence electronic structure by substituting Ir ($\lambda_{\text{SOC}} \sim 0.4$ eV [9–11]) with Ru and Rh ($\lambda_{\text{SOC}} \sim 0.19$ eV [12–14]). While these substituents have similar values of λ_{SOC} , they are electronically quite different: Ru sits to the left of Rh in the periodic table and therefore has one less electron. We will show through cluster tight-binding models that this leads to a pronounced contrast in the consequences of Rh and Ru substitution: the large impurity potential associated with Ru, inhibits hybridization with Ir, precluding a significant re-

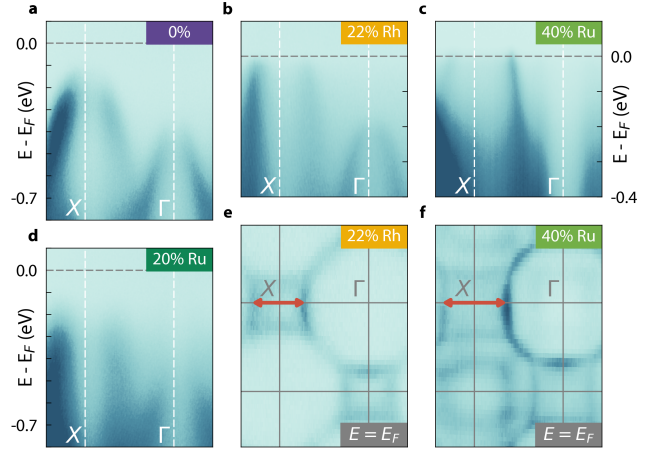


FIG. 1. **Dependence of the MIT on Rh and Ru substitution.** **a-d** ARPES spectra along $\Gamma - X$ for the pristine sample, $x_{\text{Rh}} = 0.22$, $x_{\text{Ru}} = 0.40$ and $x_{\text{Ru}} = 0.20$, respectively. **e** and **f** show Fermi surface maps for $x = 0.22$ Rh and $x = 0.40$ Ru. The relevant sizes of the pockets are indicated with red arrows. Fermi surface maps are integrated over 50 meV. Photon energy for all EDCs was $h\nu = 64$ eV with temperatures between 120 K and 150 K for $x \leq 0.10$, and below 40 K otherwise.

duction of the valence SOC. By comparison, Rh is electronically more compatible with Ir, facilitating a more successful dilution of SOC. We measure this evolution directly, through orbital mixing imbued by SOC, manifest experimentally in the photoemission dipole matrix element. To comprehend all aspects of the MIT we observe for both Rh and Ru substitution, we consider individually the effects of filling (Fig. 1), correlations (Fig. 2), and spin-orbit coupling (Figs. 3 and 4), ultimately concluding that the transition in Rh-substituted Sr_2IrO_4 is a spin-orbit controlled MIT.

[15]

Having highlighted the three relevant aspects of the MIT we will investigate, we begin our disquisition by showcasing the changes both substituents introduce to the electronic structure of the different compounds as measured by ARPES. Fig. 1a-d show ARPES spectra for $x = 0$, $x_{\text{Rh}} = 0.22$, and $x_{\text{Ru}} = 0.20, 0.40$. As reported previously [2], the pristine

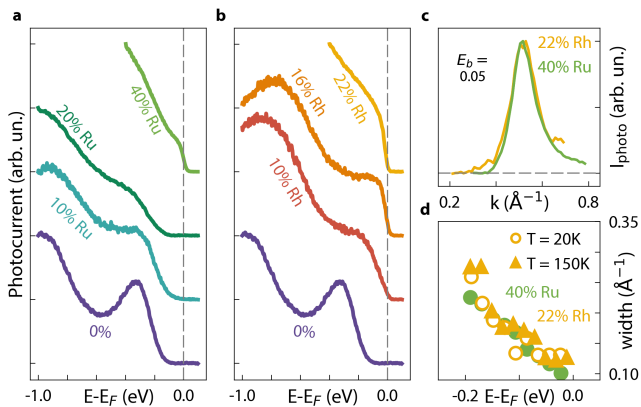


FIG. 2. ARPES linewidth evolution with substitution. Energy distribution curves (EDC's) for Ru **a** and Rh **b** substituted samples, taken at the momentum with the leading edge closest to the Fermi energy. Photon energies and temperatures for the EDCs are the same as in Fig. 1 **c** Momentum distribution curve (MDC) curves for $x_{\text{Ru}} = 0.40$ and $x_{\text{Rh}} = 0.22$. **d** MDC fits for $x_{\text{Ru}} = 0.40$ and $x_{\text{Rh}} = 0.22$. MDC data shown in **c,d** were taken using $h\nu = 92$ eV at a temperature of 20 K.

sample shows an energy gap, with a band maximum at X at a binding energy of around $E_b = 0.25$ eV. When substituting Rh, a pseudo-gapped metallic state forms for concentrations $x \gtrsim 0.13$ [6–8]. This is exemplified by our $x_{\text{Rh}} = 0.22$ data, shown in Fig. 1b and 1e. Somewhat surprisingly, the shift of the pockets for the Rh samples shown in Fig. 1b and 1e confirms its effect on filling as reported [16, 17]. The pocket size we observe for Rh seems compatible with other work, which determines the change in filling as 1 carrier per Rh [8]. At comparable values of x_{Ru} , the system remains insulating (cf. $x_{\text{Ru}} = 0.20$ in Fig. 1d), and only by going as high as $x_{\text{Ru}} = 0.40$ (Fig. 1c, 1f) do we observe the MIT has been traversed. This slower onset of metallic behavior is consistent with other reports [18, 19]. The size of the Fermi surface in Fig. 1f corresponds well to that of 0.4 holes per transition metal atom, confirming the expected filling change for a substituent that is d^4 in a lattice of d^5 ions, corroborating the suggestion of a 4+ valence for Ru sites [15]. This indicates that both Ru and Rh act as the source of one hole carrier, providing in principle similar levels of filling control at a given concentration. However, the critical concentrations at which the MIT occurs for the two species differs considerably, precluding the viability of a description in terms of an FC-type transition [6–8].

Despite the discrepancy between the critical concentrations of Ru and Rh, the correlated metallic phase which ultimately emerges share strong similarities. The energy distribution curves (EDCs) plotted cut through the valence band maximum for each doping in Fig. 2a (Ru) and 2b (Rh) reflect the evolution of each material across the MIT. From our data we infer the critical concentrations to be $x_{\text{Rh}} = 0.13 \pm 0.03$ and $x_{\text{Ru}} = 0.3 \pm 0.1$, which matches previous photoemission work on the Rh substituted compound [6–8] (Ru-substituted sam-

ples have not previously been studied by photoemission). The stark contrast of the transition concentrations is seen clearly in consideration of the two panels. While a broadening of EDC linewidth is observed with increasing concentration in both cases, the interpretation of EDC lineshapes is non-trivial [20]. We then turn to an analysis of momentum distribution curves (MDCs) for a more quantitative analysis of the evolution of correlation effects.

The MDC linewidth is directly related to the state lifetime, and by extension to both electronic interactions and disorder [21–23]. Two representative MDCs are shown in Fig. 2c for $x_{\text{Rh}} = 0.22$ and $x_{\text{Ru}} = 0.40$. Widths from these, and other MDCs along the dispersion are summarized in Fig. 2d. As can be inferred by comparison of data from 20 K and 150 K, correlations, rather than thermal broadening, are the limiting factor in determining the MDC linewidth. Consideration of both $x_{\text{Ru}} = 0.40$ and $x_{\text{Rh}} = 0.22$ reveal remarkably similar interaction effects in the two compounds, despite their significant differences in composition and disorder.

We have thus determined that while doping effects are equal to one hole per Ru/Rh, similar correlated metallic phases are observed at very different concentrations. To rectify this apparent contradiction, one must consider the context of the present MIT: it has been proposed that the correlated insulating phase in Sr_2IrO_4 is stabilized by the strong spin-orbit coupling. This motivates consideration of the role SOC plays in the MIT for both Ru- and Rh- substituted compounds. The low-energy influence of SOC can be characterized by an effective value in the valence band, determined by the hybridization between atomic species as demonstrated in [24, 25]. This effect could cause a reduction of SOC effects in the valence band as a function of (Ru,Rh) substitution. Hybridization between species is however highly dependent on the orbital energies of the substituted elements. In light of the reported electronic phase separation for the Ru compound [26–28], this suggests that such dilution of SOC may be more effective for Rh, providing a natural explanation for their contrasting critical concentration in substituted Sr_2IrO_4 compounds.

This heuristic argument can be validated quantitatively through consideration of substituted cluster models. Working within the density-functional theory, at $x = 0.25$ substitution, we observe good overlap between the Rh and Ir density of states (DOS) (Fig. 3a), allowing for proper hybridization of the electronic states. This can be compared against the same scenario with Ru in Fig. 3b, where the substituent DOS is found to align poorly with Ir. The Ru bands are offset by approximate 0.3 eV, an effect that has been reported previously for similar substitutions [29, 30]. This establishes a reasonable parameterization with which to explore the influence of doping on SOC effects in more detail. This is carried out through development of a cluster tight-binding model. We expand a single iridium basis (see Supplementary Information) to a large lattice cluster, assigning a randomly distributed fraction x of sites as substituent atoms. Within this framework, the substituents can have different λ_{SOC} (0.19 eV for both Rh and Ru) and on-site energy ($\epsilon_i = 0.0$ eV for Rh, 0.3 eV

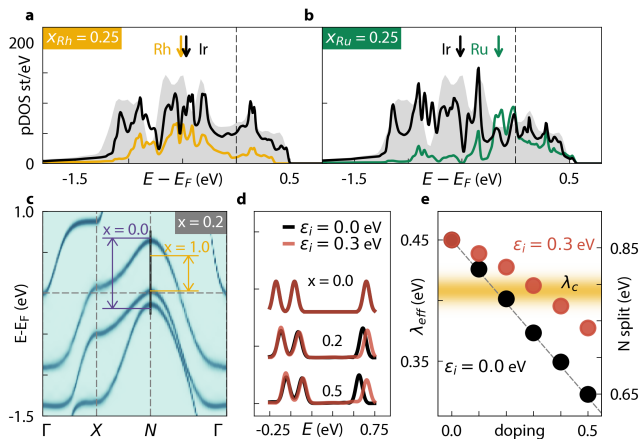


FIG. 3. Reduction of SOC through cluster analysis. **a** and **b** Analysis of the impurity potential of Rh and Ru in Sr_2IrO_4 as calculated by density-functional theory. The grey background shows the Ir projected DOS for the pristine sample. The black curves show the Ir projected DOS in the 25% substituted calculation, while the orange and teal colored curves show the projected DOS for Rh and Ru respectively. The arrows indicate the center mass for the projected bands. **c** Cluster calculated spectrum for $x = 0.2$ obtained after unfolding. The splitting at the N point for the pure end members ($x = 0.0$ and $x = 1.0$) are indicated. **d** Cuts at N (EDCs) for different concentrations of dopants. Simulations with (without) added ionic potential are shown in red (black). **e** Progression of the splitting between the outmost peaks for simulations shown in **d**; also indicated in grey is a linear interpolation between the end members of the phase diagram, which exactly matches the black markers. The orange shaded area indicates the inferred λ_c .

for Ru). The remaining sites in the cluster represent Ir with $\lambda_{\text{SOC}} = 0.45$ eV. In an effort to focus on the effects of SOC and impurity potential, kinetic terms remain the same for all sites. Similarly, octahedral distortions and electron correlations are neglected to better illustrate the shift of the j_{eff} states. We have used the unfolding method [31–34] to fold bands into the original Brillouin zone. By averaging the resulting spectral function over many random cluster configurations, we observe a smooth evolution of SOC effects in this system which depends strongly on the impurity potential.

The results are summarized in Fig. 3, with a representative unfolded spectrum ($x = 0.20$) plotted in Fig. 3c. The level spacing at the N point, indicated by the vertical arrows, is found to be a reliable measure of the valence SOC. This is seen clearly in Fig. 3d, where we present a series of EDCs along the N direction, for models with a non-zero on-site impurity potential (Ru, red), and those without (Rh, black). This doping dependence is summarized in Fig. 3e. The right vertical axis shows the splitting observed at the N point, and the left the value of spin-orbit coupling that would produce the corresponding splitting at N in a single-atom model. This second axis serves to show the effective spin-orbit coupling caused by substitution of Ir with Rh and Ru. From the progression in Fig. 3e it is evident that Rh dilutes SOC more efficiently than Ru: the black markers trace the interpolation

between the values of Ir and Rh which is shown as a dashed line. Meanwhile the impurity potential associated with Ru prevents substantial hybridization, and consequently dilution of SOC. The results in Fig. 3e suggest that the different critical concentrations for the two substituents can be attributed to a common parameter: a value for spin-orbit coupling of $\lambda_c \sim 0.41$ (indicated as an orange shaded area in Fig. 3e) yields critical concentrations ($x_{\text{Rh}} \sim 0.15$ and $x_{\text{Ru}} \sim 0.3$) that fit well with our observations. Moreover, theoretical results presented in [35] suggest that SOC in Sr_2IrO_4 is only marginally above the threshold for the insulating state, and that a small change could drive the transition. The dilution of spin-orbit coupling is therefore found to provide a compelling theoretical picture of the transition.

Having demonstrated this evolution of SOC via substitution and its ability to provide a natural explanation for the transition, we aim to substantiate these claims experimentally. To establish a convenient metric for SOC, we leverage the symmetry constraints of the photoemission matrix element. Dipole selection rules allow transitions from only certain orbitals: since d_{xz} (d_{yz} , d_{xy}) is even (odd) in the experimental scattering plane, states composed of this cubic harmonic are only observable with π - (σ)-polarization. As SOC mixes these orbitals into linear combinations prescribed by the j_{eff} construction [2], we quantify SOC by comparing the ratio of even/odd states at strategically chosen points in the Brillouin zone where these symmetry-based selection rules are most well defined. In the absence of SOC, the state along $\Gamma - X_x$ in Sr_2IrO_4 would be of pure d_{xz} character: any photoemission from this state using σ -polarization must be due to the admixture of d_{yz} and d_{xy} introduced by SOC. More quantitatively, of interest here is the value of M_x^σ , which we normalize in experiments through division by M_y^σ . A simulation of this quantity based on an *ab-initio* tight binding model for Sr_2IrO_4 with variable spin-orbit coupling is shown in Fig. 4e. The model takes into account effects of geometry as well as photon energy and polarization; for further details refer to the Supplementary Information. The curve shows a clear decrease of M_x^σ/M_y^σ as a function of spin-orbit coupling, demonstrating the possibility for a direct measure of λ_{SOC} via ARPES.

Motivated by the results of the cluster simulations, we investigate the progression of M_x^σ/M_y^σ experimentally in a series of Rh and Ru substituted samples. In Fig. 4a-d we plot constant-energy contours for each of the concentrations, as recorded with σ - polarized light. To compare the different samples, we take our constant energy maps at that energy which places the state of interest at $k = 0.75\pi/a$. Taking advantage of the nearly vertical dispersion the data has been integrated over a window of 150 meV around this energy to improve the statistical accuracy of our analysis. Integrating the ARPES intensity within the indicated regions of Fig. 4a-d yields the ratio M_x^σ/M_y^σ .

We can then proceed to make a quantitative connection with an effective spin-orbit coupling strength. To this end, we return to the previous discussion around Fig. 4e, which plots the simulated ratio as a function of spin-orbit coupling. To pro-

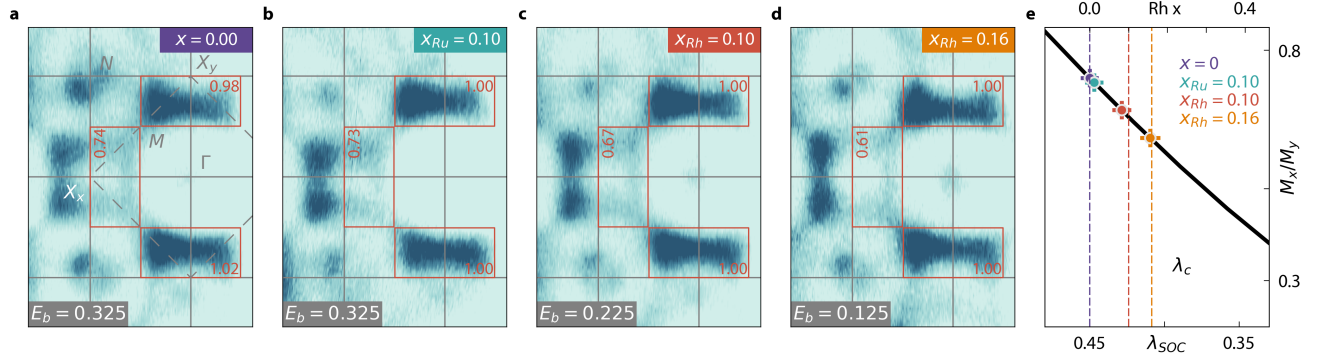


FIG. 4. Observation of the reduction of SOC via the ARPES dipole matrix element. **a-d** Constant energy maps for different concentrations of x_{Rh} , using σ -polarized light. The constant energy maps are integrated over 150 meV to improve numerical accuracy, and taken at an energy such that the size of the pocket around X is the same for all concentrations. The relevant states used for the analysis are indicated using the red boxes, and their integrated values are shown within. All data are taken at 64 eV, with temperatures at 120 K for $x = 0$ and $x_{Ru} = 0.1$, 70 K for $x_{Rh} = 0.1$, and 20 K $x_{Rh} = 0.16$, all chosen to mitigate the effects of charging. **e** Calculated ratio of matrix elements for a model of Sr_2IrO_4 (details in the Supplementary Information), plotted as a function of spin-orbit coupling, by taking a weighted average of the λ_{SOC} values of Ir ($\lambda_{SOC} = 0.45$) and Rh ($\lambda_{SOC} = 0.19$).

vide further context for these results, we normalize this curve to connect the simulation at $\lambda_{SOC} = 0.45$ with the experimental result from pristine Sr_2IrO_4 (see Supplementary Fig. 1). The remaining points can then be compared directly to a SOC strength by matching the observed M_x^σ/M_y^σ ratios to those of the normalized curve. The data suggests values of $\lambda_{SOC} = 0.443, 0.424,$ and 0.408 extracted from the measured spectra for $x_{Ru} = 0.10, x_{Rh} = 0.10,$ and 0.16 respectively. Our cluster simulations in Fig. 3 predict that for Rh λ_{SOC} should linearly interpolate the end values of $\lambda_{Ir} = 0.45$ and $\lambda_{Rh} = 0.19$. To verify the validity of this, a second axis was added that reflects the Rh concentration which would yield the corresponding interpolated λ_{SOC} . These calculated concentrations are found to agree remarkably well with those determined by electron probe microanalysis. While the Ru datapoint can not be projected in a meaningful way onto the Rh-axis scale, it aligns well with the red points in Fig. 3e at $x_{Ru} = 0.10$.

Let us now turn back to the question of the role of spin-orbit coupling in the metal insulator transition in $Sr_2Ir_{1-x}T_xO_4$ ($T = Ru, Rh$). As laid out in Figs. 1 and 2, the difference in critical concentration between Ru and Rh doped samples is unexplained by effects of filling. Using cluster simulations, we have presented the suggestion that dilution of spin-orbit coupling by substitution of different species gives rise to a natural explanation of the different critical concentrations. The impurity potential for Ru results in less hybridization and therefore less efficient dilution of spin-orbit coupling. The predicted critical concentration for Ru is therefore about twice that of Rh, which explains the dichotomy in critical concentration for the MIT to occur. The experimental results presented in Fig. 4 show that a reduction of SOC is indeed

observed with increasing concentration of Rh, and that this reduction does not occur when substituting Ru. To quantify the transition point, the $\lambda_c = 0.41$ inferred in the discussion of Fig. 3e has been added to Fig. 4e. This shows the SOC reduction is set to surpass the critical value $\lambda_c = 0.41$ at a concentration of around $x_{Rh} \sim 0.15$, in line with our experimental values. We also note that due to the complex progression of valence, the precise value of this parameter is likely related to the concurrent changes in filling and local Coulomb interactions in this system.

The combination of SOC sensitive techniques and the comparison of Ru and Rh substituted samples has therefore put us in a unique position to comment on the role of SOC in the metal-insulator transition of Sr_2IrO_4 . In our comparison of different factors including filling, correlations, and SOC, the only parameter that yields a satisfactory explanation for the dichotomy in critical concentration between Ru and Rh is spin-orbit coupling itself. We therefore conclude that spin-orbit coupling is essential to the transition. In this way we have demonstrated for the first time a spin-orbit coupling controlled collapse of a correlated insulating phase. Moreover, by demonstrating the essential role of SOC in driving the MIT, the significance of SOC in the insulating phase is directly implicated. This establishes the definitive confirmation of Sr_2IrO_4 as a relativistic Mott insulator as an important corollary to our results.

Methods

Single crystals of $Sr_2Ir_{1-x}Rh_xO_4$ were grown with nominal concentrations of $x_{Rh} = 0.0, 0.10, 0.16, 0.22$ and tested with electron probe microanalysis to be within 0.01 of their nominal concentration. Crystals of $Sr_2Ir_{1-x}Ru_xO_4$

were grown with nominal concentrations of $x_{Ru} = 0.10, 0.20, 0.40$. Measurements were carried out at the SIS beamline at the Swiss Lightsource (Rh substituted samples) and at the Merlin beamline at the Advanced Lightsource (Rh and Ru substituted samples). All measurements were done on freshly cleaved surfaces, where the pressure during measurement and cleaving was always lower than $3.3 \cdot 10^{-10}$ mbar. Measurements used for inference of spin-orbit coupling values were performed with 64 eV photons, using light polarized perpendicular to the analyzer slit direction (σ -polarization). The axis rotation of the manipulator for the acquisition of the Fermi surface was parallel to the slit direction. The sample was mounted such that the Ir-O bonds ($\Gamma - X$) was aligned to this axis of rotation. Temperatures were chosen as low as possible while mitigating the effects of charging and are reported in the figure captions. A tight binding model was constructed from a Wannier orbital calculation using the Wannier90 package [36]. The Wannier90 calculations were performed on results from density functional theory calculations done with the Wien2k package [37, 38]. Cluster calculations and matrix element calculations were done using in house developed code. Further details can be found in the Supplementary Information.

Acknowledgements

This research was undertaken thanks in part to funding from the Max Planck-UBC-UTokyo Centre for Quantum Materials and the Canada First Research Excellence Fund, Quantum Materials and Future Technologies Program. The work at UBC was supported by the Killam, Alfred P. Sloan, and Natural Sciences and Engineering Research Council of Canada's (NSERC's) Steacie Memorial Fellowships (A.D.), the Alexander von Humboldt Fellowship (A.D.), the Canada Research Chairs Program (A.D.), NSERC, Canada Foundation for Innovation (CFI), and CIFAR Quantum Materials Program. The authors would like to thank A. Nocera, M. Franz and G. Sawatzky for thorough review of the manuscript and useful comments.

-
- [1] M. Imada, A. Fujimori, and Y. Tokura, *Reviews of Modern Physics* **70**, 1039 (1998).
- [2] B. J. Kim, H. Jin, S. J. Moon, J. Y. Kim, B. G. Park, C. S. Leem, J. Yu, T. W. Noh, C. Kim, S. J. Oh, J. H. Park, V. Durairaj, G. Cao, and E. Rotenberg, *Physical Review Letters* **101**, 1 (2008), arXiv:0803.2927.
- [3] B. J. Kim, H. Ohsumi, T. Komesu, S. Sakai, T. Morita, H. Takagi, and T. Arima, *Science (New York, N.Y.)* **323**, 1329 (2009).
- [4] T. F. Qi, O. B. Korneta, L. Li, K. Butrouna, V. S. Cao, X. Wan, P. Schlottmann, R. K. Kaul, and G. Cao, *Physical Review B - Condensed Matter and Materials Physics* **86**, 1 (2012).
- [5] J. S. Lee, Y. Krockenberger, K. S. Takahashi, M. Kawasaki, and Y. Tokura, *Physical Review B - Condensed Matter and Materials Physics* **85**, 2 (2012).
- [6] V. Brouet, J. Mansart, L. Perfetti, C. Piovera, I. Vobornik, P. Le Fèvre, F. Bertran, S. C. Riggs, M. C. Shapiro, P. Giraldo-Gallo, and I. R. Fisher, *Physical Review B - Condensed Matter and Materials Physics* **92**, 1 (2015), arXiv:arXiv:1503.08120v1.
- [7] Y. Cao, Q. Wang, J. A. Waugh, T. J. Reber, H. Li, X. Zhou, S. Parham, S.-R. Park, N. C. Plumb, E. Rotenberg, A. Bostwick, J. D. Denlinger, T. Qi, M. A. Hermele, G. Cao, and D. S. Dessau, *Nature communications* **7**, 11367 (2016), arXiv:1406.4978.
- [8] A. Louat, F. Bert, L. Serrier-Garcia, F. Bertran, P. Le Fèvre, J. Rault, and V. Brouet, *Physical Review B* **97**, 1 (2018), arXiv:1801.01459.
- [9] L. Mattheiss, *Physical Review B* **13**, 2433 (1976).
- [10] S. J. Moon, H. Jin, K. W. Kim, W. S. Choi, Y. S. Lee, J. Yu, G. Cao, A. Sumi, H. Funakubo, C. Bernhard, and T. W. Noh, *Physical Review Letters* **101**, 2 (2008), arXiv:0807.2136.
- [11] B. H. Kim, G. Khaliullin, and B. I. Min, *Physical Review Letters* **109**, 3 (2012), arXiv:1205.3289.
- [12] M. Haverkort, I. Elfimov, L. Tjeng, G. Sawatzky, and a. Damascelli, *Physical Review Letters* **101**, 026406 (2008).
- [13] C. Veenstra, Z.-H. Zhu, M. Raichle, B. Ludbrook, a. Nicolaou, B. Slomski, G. Landolt, S. Kittaka, Y. Maeno, J. Dil, I. Elfimov, M. Haverkort, and a. Damascelli, *Physical Review Letters* **112**, 127002 (2014).
- [14] A. Earnshaw, B. N. Figgis, J. Lewis, and R. D. Peacock, *Journal of the Chemical Society (Resumed)*, 3132 (1961).
- [15] S. Calder, J. W. Kim, G.-X. Cao, C. Cantoni, a. F. May, H. B. Cao, a. a. Aczel, M. Matsuda, Y. Choi, D. Haskel, B. C. Sales, D. Mandrus, M. D. Lumsden, and a. D. Christianson, *Physical Review B* **92**, 165128 (2015), arXiv:1508.01807.
- [16] J. P. Clancy, a. Lupascu, H. Gretarsson, Z. Islam, Y. F. Hu, D. Casa, C. S. Nelson, S. C. Lamarra, G. Cao, and Y. J. Kim, *Physical Review B - Condensed Matter and Materials Physics* **89**, 1 (2014), arXiv:arXiv:1311.0039v2.
- [17] S. Chikara, D. Haskel, J. H. Sim, H. S. Kim, C. C. Chen, G. Fabbris, L. S. I. Veiga, N. M. Souza-Neto, J. Terzic, K. Butrouna, G. Cao, M. J. Han, and M. Van Veenendaal, *Physical Review B - Condensed Matter and Materials Physics* **92**, 1 (2015).
- [18] R. J. Cava, B. Batlogg, K. Kiyono, H. Takagi, J. J. Krajewski, W. F. Peck, L. W. Rupp, and C. H. Chen, *Physical Review B* **49**, 11890 (1994).
- [19] S. J. Yuan, S. Aswartham, J. Terzic, H. Zheng, H. D. Zhao, P. Schlottmann, and G. Cao, *Physical Review B* **92**, 245103 (2015).
- [20] A. Kaminski, M. Randeria, J. C. Campuzano, M. R. Norman, H. Fretwell, J. Mesot, T. Sato, T. Takahashi, and K. Kadowaki, *Physical Review Letters* **86**, 1070 (2001), arXiv:0004482 [cond-mat].
- [21] A. Damascelli, *Physica Scripta* **T109**, 61 (2004), arXiv:0307085 [cond-mat].
- [22] S. Hufner, *Photoelectron Spectroscopy: Principles and Applications* (Springer-Verlag, Berlin Heidelberg, 1995).
- [23] G. D. Mahan, in *Electron and Ion Spectroscopy of Solids* (1978).
- [24] C. Weeks, J. Hu, J. Alicea, M. Franz, and R. Wu, *Physical Review X* **1**, 021001 (2011), arXiv:1104.3282.
- [25] J. Hu, J. Alicea, R. Wu, and M. Franz, *Physical Review Letters* **109**, 266801 (2012), arXiv:1206.4320.
- [26] S. A. Carter, B. Batlogg, R. J. Cava, J. J. Krajewski, W. F. Peck, and L. W. Rupp, *Physical Review B* **51**, 17184 (1995).
- [27] A. Glamazda, W. J. Lee, K. Y. Choi, P. Lemmens, H. Y. Choi, N. Lee, and Y. J. Choi, *Physical Review B - Condensed Matter and Materials Physics* **89**, 1 (2014).
- [28] S. Calder, J. W. Kim, A. E. Taylor, M. H. Upton, D. Casa, G. Cao, D. Mandrus, M. D. Lumsden, and A. D. Christianson, *Physical Review B* **94**, 220407 (2016).

- [29] H. Wadati, I. Elfimov, and G. A. Sawatzky, *Physical Review Letters* **105**, 157004 (2010), arXiv:1003.2663.
- [30] G. Levy, R. Sutarto, D. Chevrier, T. Regier, R. Blyth, J. Geck, S. Wurmehl, L. Harnagea, H. Wadati, T. Mizokawa, I. S. Elfimov, A. Damascelli, and G. A. Sawatzky, *Physical Review Letters* **109**, 077001 (2012), arXiv:1203.5814.
- [31] T. B. Boykin and G. Klimeck, *Physical Review B - Condensed Matter and Materials Physics* **71**, 1 (2005).
- [32] W. Ku, T. Berlijn, and C. C. Lee, *Physical Review Letters* **104**, 1 (2010), arXiv:1002.4218.
- [33] M. W. Haverkort, I. S. Elfimov, and G. A. Sawatzky, , 1 (2011), arXiv:1109.4036.
- [34] V. Popescu and A. Zunger, *Physical Review B - Condensed Matter and Materials Physics* **85**, 1 (2012).
- [35] H. Watanabe, T. Shirakawa, and S. Yunoki, *Physical Review Letters* **105**, 216410 (2010), arXiv:1009.3311.
- [36] A. A. Mostofi, J. R. Yates, G. Pizzi, Y.-S. Lee, I. Souza, D. Vanderbilt, and N. Marzari, *Computer Physics Communications* **185**, 2309 (2014), arXiv:0708.0650.
- [37] P. Blaha, K. Schwarz, G. K. H. Madsen, D. Kvasnicka, J. Luitz, R. Laskowski, F. Tran, and M. Laurence D., *WIEN2k, An Augmented Plane Wave + Local Orbitals Program for Calculating Crystal Properties*, Vol. 1 (Karlheinz Schwarz, Techn. Universität Wien, Austria, 2018).
- [38] J. Kuneš, R. Arita, P. Wissgott, A. Toschi, H. Ikeda, and K. Held, *Computer Physics Communications* **181**, 1888 (2010).